# Energy Transport in CdSe Nanocrystals Assembled with Molecular Wires

**Artjay Javier, C. Steven Yun, Joseph Sorena, and Geoffrey F. Strouse***

*Department of Chemistry and Biochemistry, University of California, Santa Barbara, California 93106*

*Received: June 24, 2002; In Final Form: October 31, 2002*

Continuous-wave photoluminescence studies on CdSe nanocrystals assembled with oligo-*p*-(phenylene-ethynylene)$_n$-dibenzylthiols ($n$ = 0,1,3) indicate long-range resonant energy transfer can be tuned by size-dependent control of the weak electromagnetic dipole−dipole coupling of the donor (molecular wire) and the acceptor (nanocrystal). These micron-scale free-standing inorganic−organic composite structures are composed of CdSe in the strongly confined regime with diameters between 2.8 nm to 8.0 nm assembled with rigid molecular wire lengths of 1.3 nm, 1.9 nm, and 3.1 nm. Evidence is presented which supports the possibility that interchain interactions of molecular wires within the assembly form two additional species that participate in the energy transfer process, dimers and aggregate excitons. Dimer states act as intermediate states for the migrating molecular exciton, and are selectively quenched by quantized CdSe electronic transitions ($1S_{3/2}-1S_e$, $1P_{3/2}-1P_e$), while aggregate excitons act as emissive excitation traps.

## Introduction

The physics of energy transfer[1] for organic[2,3] and inorganic materials,[4] as well as inorganic−organic hybrids,[5−7] has been an intensive area of investigation for several decades. Recently, it has become an active area in quantum-confined systems[8] for both pure[9−11] and applied[12] research, and the interaction of the electronic transitions in these dimensionally confined hybrid systems[13−15] has been pursued both theoretically[6,16−19] and experimentally.[20−22] The phenomenon of quantum confinement of the Wannier-Mott exciton in CdSe below its Bohr radius[23] ($a_B \sim 5$ nm in CdSe) and the Frenkel exciton in the organic system below its Frenkel radius ($a_F \sim 3$ nm for conjugated $\pi$-systems[24,25]) results in size-dependent electronic properties for nanometer-sized semiconductors[26] and conjugated organic molecules. Specifically, the absorption and luminescence characteristics of nanocrystals in the strongly confined regime is size dependent, as shown in Figure 1. This allows for a unique opportunity to tune the energies of electronic transitions in both systems, and therefore the magnitude of the interaction of electronic transitions within a composite system.

Energy transfer between the inorganic and organic components can be described both in terms of phase-coherent strong coupling and phase-incoherent weak coupling through the dipole−dipole interaction theoretically;[17,27,28] though recent experimental results suggest nanocrystalline materials and organic−inorganic hybrids are best described in the weak coupling regime.[20] This allows the application of Förster theory,[3] which typically is used at the limit of "localized oscillators" as a result of the electric dipole approximation. The use of Förster theory allows the quantum efficiency of energy transfer to be related to the spectral overlap integral, $\langle J \rangle$, a quantity that accounts for the resonant coupling of the pseudo-continuous electronic transitions of the energy donor and the energy acceptor. A caveat of the Förster theory approximation is that the magnitude of the coupling will be inversely proportional to the sixth power of the donor−acceptor separation distance. In the tightly bound composite system where the exciton is largely

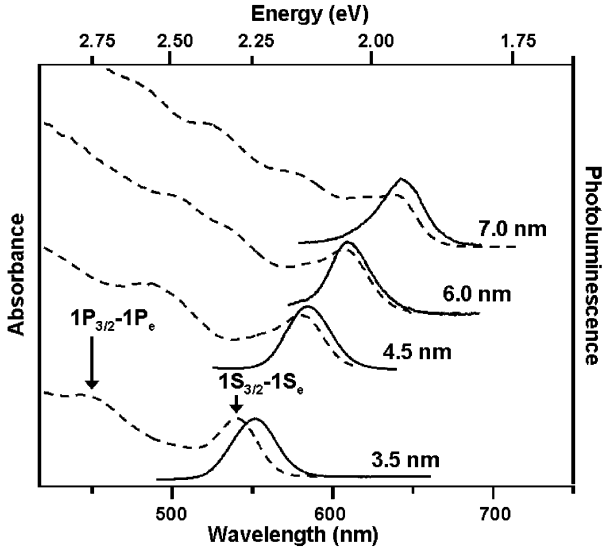


**Figure 1.** Room-temperature absorbance (dashed) and photoluminescence (solid) spectra for a series of CdSe nanocrystals coated with TOP/TOPO (diameters given at the right) in toluene. The two prominent exciton transitions are shown.

delocalized over the donor or acceptor volume, the distance will effectively be invariant for a given oligomer length, giving rise to a rate of energy transfer, and consequently an efficiency of energy transfer, dependent on the magnitude of $\langle J \rangle$. The application of the weak coupling model arises due to the dissimilarity in the wave functions of the molecular orbitals in organic systems and band-like orbitals in nanocrystals that prevents traditional strong interactions. However, strong interactions arising from exciton delocalization within the organic system due to aggregate formation may influence the pathway for energy transfer within these composites.

The $\pi$-stacking of organic systems can lead to aggregates[29] that result in a variety of new pseudo-particles that are not present in the isolated system. As these units are brought closer into contact, a critical stacking distance is surpassed (<0.7 nm) that induces drastic changes in the electronic structure of the organic system.[30,31] Interaction of two monomer units can result

* Corresponding author. E-mail: strouse@chem.ucsb.edu.

10.1021/jp0263774 CCC: $25.00 
Published on Web 12/18/2002

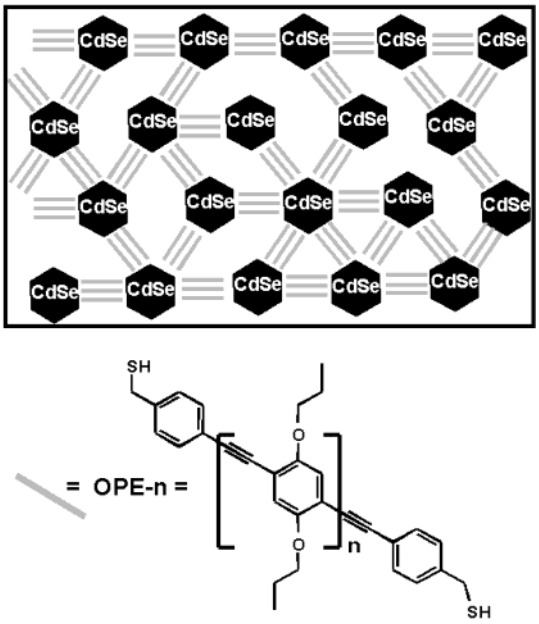


**Figure 2.** CdSe nanocrystals, coated with TOP/TOPO, form amorphous, cross-linked assemblies by ligand exchange of the phosphine by the thiol moiety when reacted with OPE-*n*: oligo-(*p*-phenylethynylene dibenzylthiol dipropyl ether) (OPE-*n*, $n = 0, 1, 3$).

in low-order exciton delocalization into simple dimers, excimers, or polaron-pairs,[32] while the participation of many monomer units can result in high-order exciton delocalization, or aggregate excitons. The new electronic transitions that arise also participate in energy transport processes and must be included in a complete description of the total energy transfer mechanism. Therefore the pathways of energy transfer in composite systems will be strongly influenced by the packing interactions of the conjugated organic system and their respective populations within that system, as these interactions give rise to the species mentioned above.

In the present study, we investigate nanocrystal composites where the photoexcited molecular wire donates energy to the nanocrystal in the form of an electronic excitation. The resonant energy transfer interaction which couples the energy donor (the molecular wire) to the energy acceptor (the nanocrystal) can be tuned in these assemblies by tuning both the length of conjugation in the molecular wire and the nanocrystal size. Moreover, dimers and aggregate excitons are present in these assemblies suggesting that these species interact with the nanocrystal exciton.

## Experimental Section

**Synthesis.** The series of oligo-*p*-(phenylene-ethynylene)$_n$-dibenzylthiols ($n = 0,1,3$) (OPE-*n*) (see Figure 2) was synthesized by a modification of literature methods.[33,34] In brief, benzylic thiol formation was achieved by the radical benzylic bromination of 4-iodotoulene followed by nucleophilic substitution with potassium thioacetate. Deprotection of the thiols was done in a basic methanolic solution, purification by column chromatography, and isolation under $N_2$, to prevent oxidation of the terminal thiol. CdSe nanocrystals between 2.8 and 8.0 nm were synthesized as TOP/TOPO passivated nanocrystals by standard lyothermal methodology.[26,35] Excess TOP/TOPO was removed by repetitive (3×) dissolution of the particles in toluene and precipitation by addition of MeOH.

**Preparation of CdSe, OPE-*n*, and CdSe-OPE Films.** CdSe-OPE films were prepared under Ar by slow addition of a 2 mL toluene solution of 0.05 M OPE-*n* to 5 mL of a 0.1 mg/mL CdSe NC in toluene at room temperature. The reaction was allowed to react 24 h under Ar, producing a solid, which was washed repeatedly with toluene to remove excess CdSe NCs and OPE, then suspended by sonication in fresh toluene for film deposition. Control experiments were conducted on OPE-*n* protected with terminal acetyl groups on the thiols.

CdSe-OPE thin films were prepared by drop casting the suspended material in toluene onto 25.4 mm wide, 0.5 mm thick circular sapphire flats. CdSe and thioacetate-protected OPE-*n* films were prepared by drop casting a mixture of CdSe and OPE-*n* in a minimum volume of toluene onto a sapphire flat.

**Electron Microscopy.** Transmission electron microscopy (TEM) analysis was performed on 400 mesh Cu grids coated with a ~5 nm layer of holey carbon (SPI). Images were obtained on a JEOL 2000 or JEOL 2010 microscope operated at 200 kV in bright field mode.

**Optical Spectroscopy.** Emission measurements were conducted on samples drop-cast onto sapphire substrates oriented either at 45° or front-face excitation using a continuous wave Omnichrome HeCd laser ($\lambda_{exc} = 325$ nm, 1 mW) with a UV filter to reject stray plasma or a 75 W Hg lamp with a 313 nm band-pass filter. The luminescence data was collected with an F/1 optic and dispersed on a CVI Instruments Digikrom 240 monochromator (150 g/mm, 10 $\mu$m slit width) coupled to a SBIG CCD model ST-6. The laser line or lamp profile was removed by a UV filter.

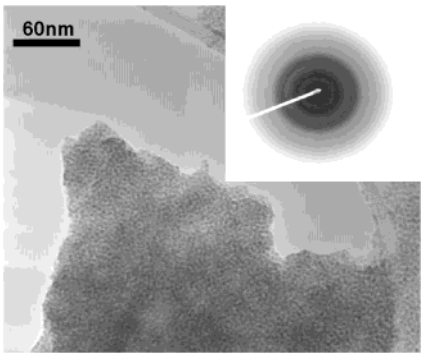


**Figure 3.** TEM of CdSe-OPE-1 assembled structures. An aggregate of CdSe-OPE is suspended over a hole in the carbon grid. Inset: SAED diffraction pattern from TEM. The observed rings indicate incorporation of wurzite CdSe into the composite without long-range ordering of the CdSe nanocrystals.

## Results

**Scaffolding of the CdSe Nanocrystals.** Slow introduction of OPE-*n* ($n = 0,1,3$) to a solution of CdSe in toluene at RT produces a solid monolith (Figure 2). TEM analysis of the CdSe-(4.5 nm)-OPE-1 monolith shows closely packed CdSe nanocrystals (Figure 3) lacking orientational order based on SAED ring patterns (Figure 3, inset). Similar observations are found for composites formed with OPE-0 and OPE-3. The phenylethynylene core of the organic oligomer which has been used for molecular wire applications[36−39] was chosen for both its rigidity and low conductivity, the latter of which enhances energy transfer phenomena by impeding the competing phenomenon of electron conduction. The placement of a methylene group between the thiol and the phenyl rings serves to interrupt the conjugation preventing photochemical redox processes at the nanocrystal surface by raising the oxidation potential of the thiol. The assembled monolith cannot be redispersed in solvent following precipitation. Optical absorption in these materials

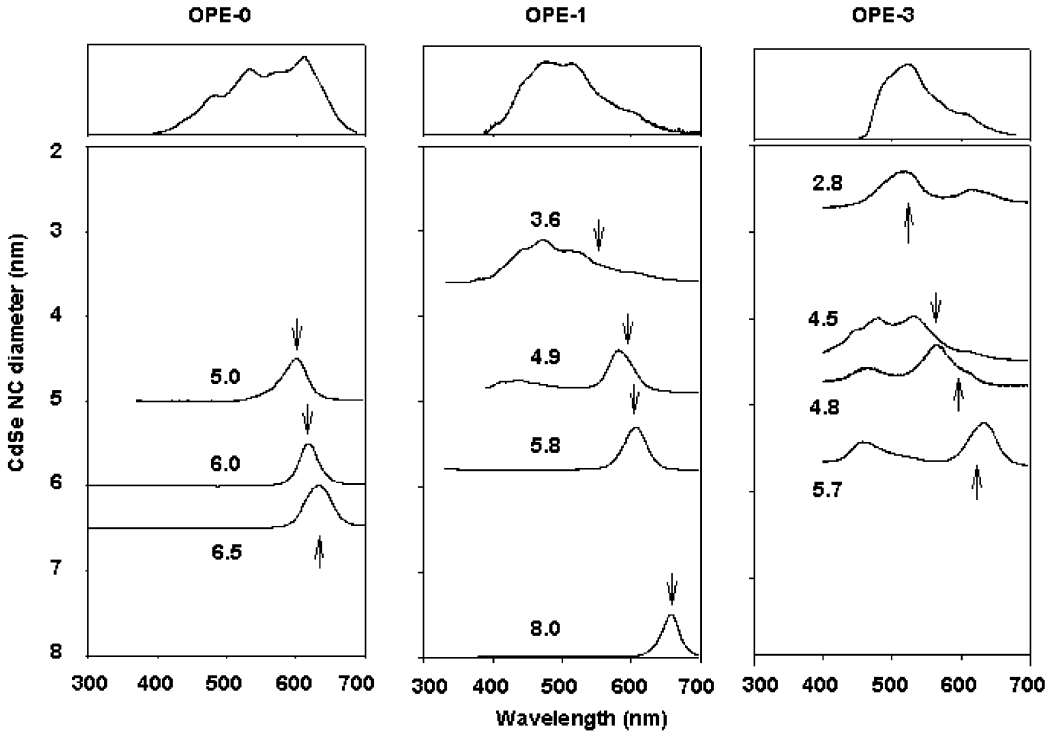


**Figure 4.** Photoluminescence spectra of thin films of OPE-*n* (top row) and CdSe-OPE-*n* assemblies at room temperature ($\lambda_{ex} = 325$ nm, ~1 mW). Columns pertain to OPE-*n* sizes ($n = 0, 1, 3$) while rows indicate CdSe NC diameters in nanometers. Arrows indicate the expected position of nanocrystal luminescence

suggests that the composite is composed of >100:1 mole ratio of oligomer to CdSe. Unfortunately, complications arising from light scattering in these solutions limit the accuracy of determination of the mole ratios using absorption measurements.

**Photoluminescence (PL) Spectra.** The PL spectra of OPE-*n* and OPE-*n*/CdSe composites when excited at 325 nm are shown in Figure 4. There is an overall trend in the reduction of the presence of the OPE-*n* luminescence relative to the nanocrystal band-edge luminescence as the nanocrystal size is increased (from top to bottom) and the oligomer chain length is decreased (from right to left). In fact, for the CdSe-OPE-0, nanocrystal emission is exclusively observed for all assemblies containing CdSe. For sizes below CdSe(4.9 nm)-OPE-1, a contribution of the PL from both the nanocrystal and OPE-1 is observed. For the CdSe-OPE-3 sample, contributions from both CdSe and OPE-3 are observed for all the CdSe-OPE-3 samples studied with strong aggregate contributions observable at 570 and 603 nm. No significant contributions from deep trap luminescence from CdSe is observed in the composite structures. In general, there appears to be an improvement in the signal/noise ratio in assemblies with increasing nanocrystal size, implying that the PL quantum yield for these are greater. Exact measurements of quantum yields have not been explicitly measured.

The change in the relative contributions of the PL of the two components is a function of nanomaterial size and OPE-*n* length. The total PL manifold can be assigned by inspection of the concentration-dependent absorbance and PL of OPE-1 (Figure 5), and the size dependent emission of the nanomaterial. Upon closer inspection of the PL manifold, changes in OPE-*n* PL are observed which appear to depend on nanocrystal size. These observations can be understood when considering the effects of interchain interactions that form dimers and aggregate interactions of OPE-*n*. At very low concentrations of ($10^{-7}$ M)−($10^{-12}$ M), the luminescence spectrum of OPE−1 arises almost exclusively from the molecular exciton, consisting of the $S_1 \rightarrow S_0$ transition and its vibronic progression (A, B). A low energy

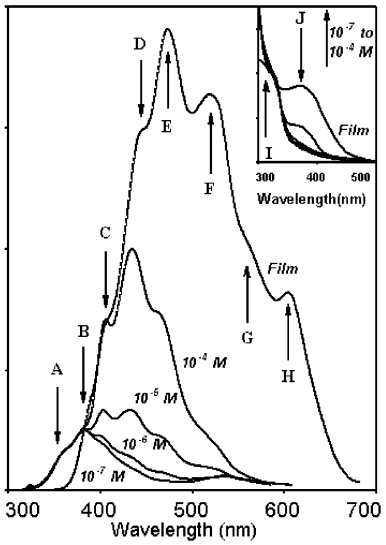


**Figure 5.** Concentration-dependent photoluminescence spectra of OPE-1 in toluene at room temperature ($\lambda_{ex} = 325$ nm, ~1 mW). Inset: Room-temperature absorption spectra of OPE-1 in toluene at the corresponding PL concentrations. Note that both have been normalized to the absorption or luminescence of the molecular species.

band at 535 nm is assignable to a phosphorescent $T_1 \rightarrow S_0$ (F), giving a singlet−triplet energy difference $E_{ST} \sim 1$ eV, which is consistent with typical exchange energies in organic systems. Its strength relative to the singlet fluorescence implies significant mixing of singlet and triplet states, possibly due to increased spin−orbit coupling from the sulfurs in the thiols.

As the concentration is progressively increased, contributions from dimers begin to appear as new bands in the PL that are shifted to the red (C, D, E) along with a corresponding new band in the absorbance at 390 nm (J) that is red-shifted from the absorbance of the monomer OPE-*n* (I). Spectral subtraction of the lowest concentration PL spectrum from the higher

concentration PL spectra reveals an emission manifold that is structured. This implies that as the concentration is increased, a new species with distinct vibronic structure (C, D, E) is formed with the coincident decrease in the contribution from the isolated OPE-*n*. The presence of the new absorbance band (J) with increasing concentration implies a ground-state dimer is being formed, but since it is not directly being photoexcited, the luminescence must come from the migration of the energy of the molecular exciton to these dimer states via energy migration. PL excitation spectra of the new bands in the PL overlay very well on the absorbance, especially band J, indicating that these dimer states are the source of the new luminescence. Changes in the relative intensities of these bands in the absorbance spectra with respect to concentration suggest aggregate formation arising from $\pi$-stacking effects between OPE-*n* molecules.

When OPE-*n* is cast as a film, contributions from higher-order aggregates arise at lower energy as seen in Figure 5 (G, H). It can also be seen from the PL that the bands originating from the molecular species are no longer present, suggesting in the film the observed PL arises primarily from dimeric species and aggregate bands. The presence of the OPE-*n* molecular species in the absorbance of the film suggests facile exciton migration to the dimers and aggregates following excitation of the OPE-*n* molecule. No noticeable band structure evident in the film absorbance accounts for the new aggregate peaks (G, H) found in the luminescence. Similar aggregate spectra arise in PPE, the polymeric variant of the oligomer being studied.[40]

These results suggest that exciton states exist in this system that can be described as being delocalized over a larger volume due to interchain interactions[41] and therefore may serve as low energy emissive traps. The actual interaction involves cofacial alignment of planar $\pi$-systems[31,42,43]which causes a splitting of the molecular orbitals,[30,31,43] resulting in a symmetry-forbidden lowest energy excited-state recombination. Electron−phonon coupling[44] or misalignment relaxes the selection rule, allowing radiative decay of the lower state which results in a red-shift in the luminescence. Aggregate states can be described as an extension of this model to larger numbers of participating units, causing the energy splitting to be much greater, and therefore to be more red-shifted, just as we observe in the OPE-1 film. The acetyl-protected OPE-*n* also displays new luminescence features when cast into a film. The spectral differences between the protected and unprotected versions can be explained as a sensitivity of aggregate states to their packing arrangement, which in other studies has been found to strongly depend on many factors, even film preparation.[45]

As stated earlier, when OPE-*n* is assembled with CdSe, we observe changes in the OPE-*n* PL spectrum that are dependent on CdSe size. We can group these changes into three observations: (i) the aggregate bands (G, H) appear in these assemblies regardless of the CdSe size used, (ii) the dimer bands (C, D, E) of OPE-*n* appear in the smallest CdSe sizes (2.8, 3.6 nm), but are not present in the intermediate and larger sizes, (iii) the OPE-*n* molecular luminescence (A, B) appears in the intermediate CdSe sizes only (4.5, 5.5 nm) and not in larger or smaller sizes. Another noticeable result is that the triplet band is not present in the larger nanocrystal sizes (5.0 nm in OPE-1), implying that this OPE-*n* excited state is also coupled to the nanocrystal. These effects are all indicative of a complicated mechanism involving the interactions of individual OPE-*n* excitations with the size-dependent electronic transition energies of the nanocrystal. To understand how OPE-*n* interacts with these changes, we employ the simplest model involving the interaction of the OPE-*n* molecular exciton with the nanocrystal, and apply the simplest mechanism, Förster energy transfer. We will later use this model to provide some insight into the interaction between dimer states and aggregate states with the nanocrystal.

## Discussion

**Energy Transfer (Simple Förster Model).** Electronic energy transfer in these materials originates from a transition dipole−dipole interaction between the many discrete transitions of the organic oligomer, OPE-*n* and its aggregates to the discrete and continuum-like states of the nanomaterial. The nature of the interaction can be described in terms of a strong or weak coupling regime between the donor and acceptor states.[3] The amorphous nature of the inorganic−organic hybrid structure for CdSe-OPE-*n* structures with respect to nanocrystal orientational order (Figure 3, inset), the inhomogeneous distribution of CdSe sizes resulting in nonidentical potential wells, the lack of periodicity, and the resulting dissimilar discrete transition energies between the CdSe and OPE-*n* eliminates the strong coupling regime. In the weak coupling limit, the resonant energy is irreversibly transferred from the donor to the acceptor due to the lower-lying acceptor electronic transition acting as an energy trap. Assuming vibrational relaxation occurs faster than energy transfer (a result of being in the weak limit) the energy transfer mechanism can be described as a combination of Coulombic (Förster mechanism) and exchange (Dexter mechanism) interactions. The strength of the exchange interaction drops off exponentially with respect to the donor−acceptor separation distance, and is only a major contributor to the total energy transfer if all other resonant transitions are forbidden. Therefore, in this case, the energy transfer should be well described in a limiting condition as a Coulombic interaction between the electronic system of the donor and the electronic system of the acceptor. Observation of the aggregate states in the spectrum confirm the facile relaxation to the lowest organic levels prior to energy transfer, supporting the weak coupling approximation. Within this mechanistic framework, two competitive models exist that describe energy transport, Förster's model involving localized dipole oscillators and an exciton diffusion model. It is likely that the Förster model is the more applicable model due to the short lifetimes of CdSe trapping the excitation more efficiently and the lack of very long-range crystalline domains, effectively reducing exciton mobility. A time-resolved study on a system similar to ours suggests exciton diffusion may play a role in describing the energy transfer mechanism,[20] though this may be due to contributions arising from aggregates, as discussed later.

In the CdSe-OPE-*n* system, with a fixed donor−acceptor distance, the very strong oscillator strengths of the OPE-*n* and CdSe transitions indicate that the energy transfer process is dominated by the strength of the resonant coupling energy, quantified as the spectral overlap integral $\langle J \rangle$.

$$\langle J \rangle = \int_0^\infty F_D(\lambda)\lambda^4 \epsilon_A(\lambda)\, d\lambda \qquad (1)$$

where $F_D$ is the normalized fluorescence intensity of the donor, and $\epsilon_A$ is the molar extinction coefficient of the acceptor. According to Förster's theory,[46] the rate of energy transfer ($k_{EnT}$) is

$$k_{EnT} = \frac{9000(\ln 10)}{128\pi^5} \frac{\kappa^2 \Phi_D}{\eta^4 N_A r^6 \tau_D} \langle J \rangle = \frac{A}{\tau_D} \langle J \rangle \qquad (2)$$

where $r$ is the distance between the donor and acceptor dipoles, $\Phi_D$ and $\tau_D$ are the native quantum yield and lifetime of the donor, respectively, $\kappa$ is the relative orientation of the donor and acceptor dipoles, $\eta$ is the refractive index of the medium, and $N_A$ may be correct in preprint. We estimate the orientation factor $\kappa^2 = 2/3$, consistent with an isotropic orientation of transition dipoles within the assembly, which is reasonable considering the disorder in nanocrystal orientation observed in the SAED spectrum in Figure 3. For the CdSe-OPE-$n$ system, we have grouped invariant terms for a given organic donor into $A$, leaving $k_{EnT}$ to be directly proportional to $\langle J \rangle$. The quantum efficiency of energy transfer ($\Phi_{EnT}$), an experimental observable, can be expressed as a ratio of the rate of energy transfer ($k_{EnT}$) to the sum of the rates of all processes that deactivate the excited state ($\Sigma k_i$):

$$\Phi_{EnT} = \frac{k_{EnT}}{\sum_i k_i} = \frac{k_{EnT}}{k_{EnT} + \frac{1}{\tau_D}} \quad (3)$$

The quantum efficiency of energy transfer ($\Phi_{EnT}$) in terms of $\langle J \rangle$ in these hybrid nanocomposites can then be expressed by substitution of (eq 2) into (eq 3):

$$\Phi_{EnT} = \frac{\langle J(R) \rangle}{\langle J(R) \rangle + A^{-1}} \quad (4)$$

This allows the rate ($k_{EnT}$) and efficiency ($\Phi_{EnT}$) of energy transfer to be interpreted entirely by analysis of the spectral overlap integral, which, holding all else constant, is entirely dependent upon CdSe size ($R$). This occurs because $\langle J \rangle$ is a complicated function of the nanocrystal size. For example, if we consider only the $1S_{3/2}-1S_e$ transition, we find that the magnitude of the extinction coefficient in CdSe is proportional to the volume ($\sim R^3$)[47] and that the energy of the transition is proportional to the inverse square of the radius ($\sim R^{-2}$).[23] The higher-order transitions also follow a similar trend though their oscillator strength is not as large.[48] $\langle J \rangle$ increases with increasing nanocrystal size due to the greater overlap of $\epsilon_A(\lambda)$ with $F_D(\lambda)$, and consequently, the rate of energy transfer also increases.

Figure 6 shows the OPE-$n$ molecular exciton energies relative to the lowest energy CdSe discrete ($1S_{3/2}-1S_e$, solid line) and other higher-order and continuous transitions (gray bar) with different CdSe sizes. The OPE-$n$ molecular exciton is always resonant with some CdSe electronic transition, but the dimer states progressively increase in their overlap with CdSe as the size increases, which would in turn lead to greater energy transfer from those states. As the CdSe size is increased above 3 nm, the nanocrystal exciton ($1S_{3/2}-1S_e$) becomes resonant with the OPE-$n$ dimer exciton, and energy transfer is predicted to be more efficient. As the CdSe size is increased further, the $1S_{3/2}-1S_e$ nanocrystal exciton is no longer resonant, but OPE-$n$ dimer states remains resonant with other higher energy excitons, as well as a higher density of continuum states, contributing to a general increase in the energy transfer as a function of size. A similar effect occurs for the aggregate states, but at much larger CdSe sizes. Plots of the spectral overlap integral $\langle J \rangle$ more clearly illustrate this, as shown in Figure 7. Inspection of the calculated value of $\langle J \rangle$ using the OPE-$n$ protected film luminescence with different nanocrystal extinction spectra (Figure 7) reveals that the smallest CdSe sizes show an overlap of the blue edge of OPE-$n$ with the red edge of CdSe(2.8 nm).

As the CdSe size is increased, the decrease in the CdSe band gap causes all of the transitions to shift toward the red,

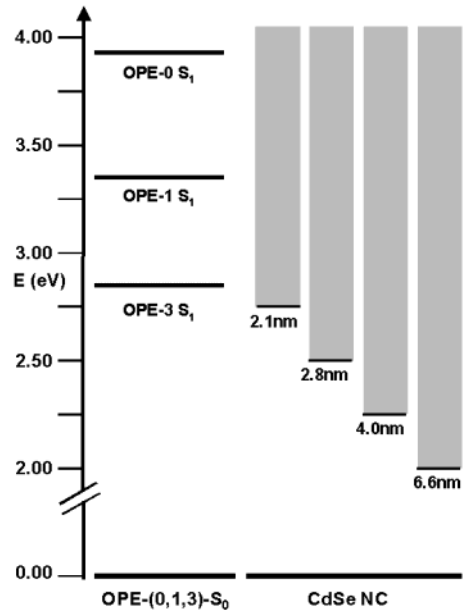


**Figure 6.** Excitation energy diagram for OPE (left) and CdSe (right). The electronic excitation energies of the singlet states have been estimated from the crossing of the absorption and luminescence curves. The exciton energy for the ($1S_{3/2}-1S_e$) has been estimated from the exciton maximum in the absorbance spectrum, and is shown along with the continuum of gap states.

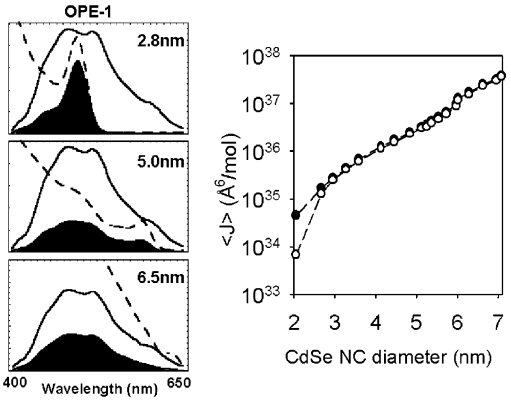


**Figure 7.** Left: The luminescence of OPE-1-protected film, the absorption of CdSe in toluene at 298 K, and the spectral overlap integral (filled in) for three representative sizes of CdSe. Top: Plot of $\langle J \rangle$ for OPE-1 (closed circles) and OPE-3 (open circles).

overlapping with more OPE-$n$ states, until in the largest size of CdSe (CdSe(6.5) also seen in Figure 7) the entire OPE-$n$ luminescence is resonant with either discrete transitions in CdSe or the continuum of band gap states. This allows the trend in the magnitude of the relative emission in Figure 4 to be analyzed by consideration of the size-dependent change in the spectral overlap integral between the OPE-$n$ and the CdSe nanomaterials. For a given family in Figure 4, the QD/oligomer concentrations were kept constant; however, the exact concentrations in the final assemblies are difficult to assess. As the spectral overlap increases, an increase in quenching of the OPE-$n$ PL is expected with a corresponding increase in the nanocrystal PL contribution. Förster theory therefore predicts a relative increase in the ratio of CdSe band-edge luminescence to OPE-$n$ luminescence with increasing nanocrystal size (moving vertically downward in Figure 4) and decreasing OPE-$n$ chain length (moving horizontally to the left in Figure 4). There are many factors that change dramatically as one moves horizontally in Figure 4, including the separation distance and the excited-state lifetime.

Although Förster's theory has an exact distance dependence, it is only explicit for distances that are greater than the donor and acceptor dimensions. That is, both the nanocrystal and OPE-*n* excitons are delocalized across their volumes and are at very close proximity, effectively blurring the exact separation distance. At the relatively short donor−acceptor distances used in these assemblies, the distance dependence of the energy transfer is not expected to be significant.

The simple Förster model discussed above describes an average interaction between OPE-*n* and CdSe. This model, however, does not account for the difference in the luminescence intensity ratios between CdSe-OPE-1 and CdSe-OPE-3, nor does it account for the change in the OPE-*n* manifold as the nanocrystal size is increased. $\langle J \rangle$ values between *different* OPE-*n* ligands with the *same* nanocrystal size are very similar, which suggests that another mechanism is responsible for the noticeable change in luminescence when switching organic systems that is unrelated to the resonant interaction between OPE-*n* and CdSe. This may be attributed to a number of different factors including luminescence lifetime, changes in extinction coefficient, and especially differences in packing environments on the nanocrystal surface, all of which may contribute to the resulting luminescence. Part of the answer lies in the aggregate species that are present as a result of OPE-*n* interactions with itself. It should be stressed that the calculations for $\langle J \rangle$ are made with the solid-state luminescence spectra of the OPE-*n*, which has contributions from aggregates whose populations will differ in the assemblies. In the CdSe-OPE-*n* assemblies, the aggregate populations will be disturbed by the nanocrystal presence due to changes in the packing interactions. This results in a distortion of the OPE-*n* luminescence data due to the differences in orientation or different micro-environments of the OPE-*n*, which lead to changes in the energy transfer.

**Contributions from Higher-Order $\pi-\pi$ Interactions.** The spectral changes that accompany the quenching in these assemblies are suggestive of aggregate and dimer participation in the energy transfer. While these assemblies are generally amorphous with respect to nanocrystal placement, the presence of local dimers and aggregate conformations within the assemblies can be inferred from inspection of the PL spectra. Luminescence from higher-order structures is clearly visible in the PL spectra of the assemblies in nearly every size nanocrystal and may cause some distortion to the nanocrystal band-edge luminescence in the higher sizes due to overlap, which is highly suggestive that aggregate formation of OPE-*n* occurs on the nanocrystal surface. Comparison of the PL data for the CdSe-OPE-*n* composite (Figure 4), with the PL (Figure 5) for OPE-*n* shows an apparent distortion in the remnant OPE-*n* luminescence that causes the spectrum for the OPE-*n* to shift toward the "blue," as is clearly seen in CdSe(4.8)-OPE-1 and CdSe-(4.9 and 5,7)-OPE-3. Closer inspection reveals that there is no shift, rather this occurs due to changes in the intensities of the OPE-*n* luminescence manifold composed of molecular, dimer, and aggregate excitons. The apparent shift can be interpreted as preferential quenching of the lower energy dimer-like transitions preferentially in the composite. These lower energy transitions (C, D, E) disappear with increasing nanocrystal size, and quench faster than the molecular PL (A, B), thereby causing the overall OPE-*n* luminescence to appear as though it were shifting toward the blue. This observation implies two possibilities: that the interaction between this delocalized dimeric excitation and the nanocrystal excitonic states are stronger than the molecular excitation coupled to the same excitonic states, or that increasing nanocrystal size induces less association among OPE-*n* ligands. The latter case is unlikely since larger nanocrystal sizes have larger stable crystal facets and should increase the occurrence of domains of dimer species and aggregate domains at the expense of the molecular species. We would in this case observe a reduction in the molecular luminescence with a corresponding increase in the dimer and aggregate luminescence. We observe, however, the opposite effect—the molecular luminescence grows in and the aggregate luminescence is apparently unaffected, but the dimeric luminescence decreases. In fact, aggregate bands appear quite prominently in the smallest nanocrystal sizes, implying that even at these small facet sizes, an aggregate domain can form stably. This leaves the former case, that there must exist a strong interaction between the discrete nanocrystal exciton states and the dimer state of OPE-*n*. This is not a surprising result since the rate of energy transfer in Förster theory is based upon the strength of resonant transition dipoles, and the nanocrystal oscillator strength is carried predominantly by the $1P_{3/2}-1P_e$ and $1S_{3/2}-1S_e$, which happen to be resonant with the OPE-*n* dimers over the participating nanocrystal sizes. For example, with CdSe roughly in the 4.5 to 5.5 nm range, the $1P_{3/2}-1P_e$ overlaps extremely well (∼450−500 nm) with the dimer luminescence (∼435−500 nm). It is possible that the $2S_{3/2}-1S_e$ transition also plays a role in the quenching since this transition is also resonant with the dimer states, however it is expected to be due to its resonance with the dimer states rather than its oscillator strength, which is expected to be quite low.[8]

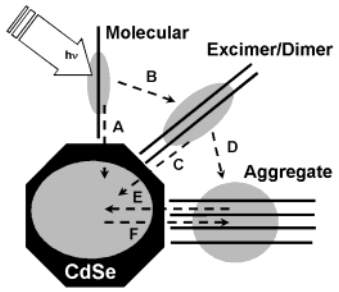


**Figure 8.** Excitation is generated as a molecular exciton which then can migrate to a dimer, delocalize into an excimer or polaron-pair, B, or delocalizes/migrates to an aggregate exciton, D. All three species, molecular exciton, excimer/dimer, and aggregate, can transfer energy to the nanocrystal (A,C,E). F is the back-transfer of energy from the nanocrystal to the aggregate.

The variance of this phenomenon between similar sizes of CdSe, such as CdSe(4.5)-OPE-3 and CdSe(4.8)-OPE-3 is due to the size-dependent changes in the discrete transition energies of the nanocrystal. We stress that the coupling to the continuum of band gap transitions would not have the same effect as these increase monotonically toward higher energies and would therefore favor the quenching of higher energy transitions such as the isolated molecular luminescence, which is the opposite of what we observe. Moreover, this effect is not seen in the lowest energy organic system luminescence, the aggregate excitons, since these are the lowest energy states of the composite system.

The occurrence of dimers and aggregates within the assemblies complicates the simple Förster model of energy transfer. Figure 8 is a schematic of the possible pathways for the electronic energy to pursue within the assembly. The excitation originates from the optical pumping of either the OPE-*n* ligand or the nanocrystal, with the former being the preferential path. Vibrational relaxation occurs first (consistent with a weak coupling model), at which point the excitation can either transfer to the nanocrystal by the Förster mechanism, or

become delocalized among different adjacent OPE-*n* ligands (the former is the preferred path). Low-order delocalization can occur to a small number of adjacent OPE-*n* ligands (dimers) or high-order delocalization can occur to a large number of OPE-*n* ligands (aggregates). These low-order delocalized states can be the dimers mentioned above, excimers, or polaron pairs,[49] formed due to photoinduced electron transfer to a cofacial molecule, which effectively delocalizes the exciton, or resonant energy transfer to dimer or aggregate states. We have little information indicating which is predominantly observed. Low-order delocalized states can transfer their energy to the nanocrystal, while the aggregate excitations need not. This occurs because the aggregate bands are found lower in energy than the nanocrystal exciton states and as a result are the lowest excitation energy states in several of these assemblies. Due to the low cross section for aggregates in the inorganic−organic composites, the number of aggregate excitons (traps) is difficult to determine directly in these materials. However, the population of aggregate states should increase with increasing chain length and nanocrystal size due to more efficient packing on a nanocrystal facet.[50] Although the concentration of aggregates is small, theory infers very fast (picosecond) Förster energy transfer from a semiconductor nanocrystal to an organic matrix.[51]

In a variety of the assemblies present, particularly those with small nanocrystal size and large OPE-*n* chain length, a back-transfer event is plausible (Figure 8, path F). In this case, an excitation originates from either a direct photoexcitation of the nanocrystal or an excitation transferred from a molecular or low-order excitation. This excitation then transfers from the nanocrystal to the aggregate exciton, whereby the aggregate exciton annihilates. This leads to the aggregate exciton as the lowest energy trap for these composite materials, but since nanocrystal disruption of long-range ordering among OPE-*n* ligands produces a very small population of aggregates, these aggregate states can be thought of as low energy trap centers.[52] A plausible case exists where the aggregate exciton migrates from aggregate domain to aggregate domain, but this event is unlikely since the aggregate domains in these assemblies are expected to be well separated.

## Conclusion

Continuous-wave PL studies show that the phenomenon of quantum confinement can be exploited to control energy transfer in inorganic−organic composites by the tuning of resonant interactions, which presumably occur through weak electromagnetic coupling. We show that there is a strong absorption of photon energy by OPE-*n* followed by a rapid energy injection to CdSe resulting in strong nanocrystal luminescence, the rate of which can be controlled by adjusting the nanocrystal size, which in turn adjusts the resonant interaction of the two. Calculations for this resonant interaction manifested in the spectral overlap integral, $\langle J \rangle$, further verifies this. Moreover, the preferential quenching of different polymer configurations implies a strong dependence of the energy transfer on the delocalization of the OPE-*n* exciton, and that discrete quantum-confined nanocrystal states interact with the delocalized excitation. We are exploring this interaction of delocalized OPE-*n* excitons and nanocrystal excitons further. Current studies are being pursued on the time dependence under continuous photoexcitation of the above OPE-*n* ligands assembled on CdSe, as well as their protected counterparts. They suggest that a photoinduced luminescence-detected chain melting originating from a possible TICT-ES (Twisted Intramolecular Charge-Transfer Excited State) influences the rate of energy transfer.

**Acknowledgment.** This work was supported by a NSF-CAREER Award (DMR-9875940). We thank Greg Khitrov for the TEM image.

## References and Notes

(1) Agranovich, V. M.; Galanin, M. D. *Electronic excitation energy transfer in condensed matter*; North-Holland Pub. Co.: Sole distributors for the USA and Canada Elsevier North-Holland: Amsterdam; New York, 1982.

(2) Turro, N. J. *Modern molecular photochemistry*; University Science Books: Mill Valley, CA, 1991.

(3) Lamola, A. A.; Turro, N. J.; Leermakers, P. A.; Weissberger, A. *Energy transfer and organic photochemistry*; Interscience Publishers: New York, 1969.

(4) Di Bartolo, B.; Karipidou, A. *Energy transfer processes in condensed matter*; Plenum Press: New York, 1984.

(5) Bassani, F.; La Rocca, G. C.; Basko, D. M.; Agranovich, V. M. *Phys. Solid State* **1999**, *41*, 701−703.

(6) Agranovich, V. M. *Uspekhi Fizicheskikh Nauk* **1999**, *169*, 348.

(7) Hranisavljevic, J.; Dimitrijevic, N. M.; Wurtz, G. A.; Wiederrecht, G. P. *J. Am. Chem. Soc.* **2002**, *124*, 4536−4537.

(8) Efros, A. L.; Rosen, M. *Annu. Rev. Mater. Sci.* **2000**, *30*, 475−521.

(9) Kagan, C. R.; Murray, C. B.; Nirmal, M.; Bawendi, M. G. *Phys. Rev. Lett.* **1996**, *76*, 1517−1520.

(10) Kagan, C. R.; Murray, C. B.; Bawendi, M. G. *Phys. Rev. B−Condens. Matter* **1996**, *54*, 8633−8643.

(11) Brongersma, M. L.; Hartman, J. W.; Atwater, H. A. *Phys. Rev. B* **2000**, *62*, R16356−R16359.

(12) Willard, D. M.; Carillo, L. L.; Jung, J.; Van Orden, A. *Nano Lett.* **2001**, *1*, 469−474.

(13) Greenham, N. C.; Peng, X. G.; Alivisatos, A. P. *Phys. Rev. B−Condens. Matter* **1996**, *54*, 17628−17637.

(14) Greenham, N. C.; Peng, X. G.; Alivisatos, A. P. *Synth. Met.* **1997**, *84*, 545−546.

(15) Huynh, W. U.; Peng, X. G.; Alivisatos, A. P. *Adv. Mater.* **1999**, *11*, 923−927, 886.

(16) Agranovich, V. M.; Basko, D. M. *JETP Lett.* **1999**, *69*, 250−254.

(17) Agranovich, V. M.; LaRocca, G. C.; Bassani, F. *Pure Appl. Opt.* **1998**, *7*, 119−127.

(18) Agranovich, V. M.; Basko, D. M.; LaRocca, G. C.; Bassani, F. *J. Phys.: Condens. Matter* **1998**, *10*, 9369−9400.

(19) Agranovich, V. M.; LaRocca, G. C.; Bassani, F. *JETP Lett.* **1997**, *66*, 748−751.

(20) Sirota, M.; Minkin, E.; Lifshitz, E.; Hensel, V.; Lahav, M. *J. Phys. Chem. B* **2001**, *105*, 6792−6797.

(21) Sirota, M.; Fradkin, L.; Buller, R.; Henzel, V.; Lahav, M.; Lifshitz, E. *Chemphyschem.* **2002**, *3*, 343−349, 314.

(22) Finlayson, C. E.; Ginger, D. S.; Greenham, N. C. *Chem. Phys. Lett.* **2001**, *338*, 83−87.

(23) Steigerwald, M. L.; Brus, L. E. *Acc. Chem. Res.* **1990**, *23*, 183−188.

(24) Knupfer, M.; Pichler, T.; Golden, M. S.; Fink, J.; Murgia, M.; Michel, R. H.; Zamboni, R.; Taliani, C. *Phys. Rev. Lett.* **1999**, *83*, 1443−1446.

(25) Knupfer, M.; Zojer, E.; Leising, G.; Fink, J. *Synth. Met.* **2001**, *119*, 499−502.

(26) Murray, C. B.; Sun, S. H.; Gaschler, W.; Doyle, H.; Betley, T. A.; Kagan, C. R. *IBM J. Res. Dev.* **2001**, *45*, 47−56.

(27) Basko, D.; La Rocca, G. C.; Bassani, F.; Agranovich, V. M. *Eur. Phys. J. B* **1999**, *8*, 353−362.

(28) Agranovich, V. M.; LaRocca, G. C.; Bassani, F.; Benisty, H.; Weisbuch, C. *Opt. Mater.* **1998**, *9*, 430−436.

(29) Collison, C.; Treemaneekarn, V.; Oldham, W. J.; Hsu, J. H.; Rothberg, L. J. *Synth. Met.* **2001**, *119*, 515−518.

(30) Cornil, J.; Beljonne, D.; Calbert, J. P.; Bredas, J. L. *Adv. Mater.* **2001**, *13*, 1053−1067.

(31) Cornil, J.; Calbert, J. P.; Beljonne, D.; Silbey, R.; Bredas, J. L. *Synth. Met.* **2001**, *119*, 1−6.

(32) Frankevich, E.; Ishii, H.; Hamanaka, Y.; Yokoyama, T.; Fuji, A.; Li, S.; Yoskino, K.; Nakamura, A.; Seki, K. *Phys. Rev. B* **2000**, *62*, 2505−2515.

(33) Huang, S. L.; Tour, J. M. *Tetrahedron Lett.* **1999**, *40*, 3347−3350.

(34) Jones, L.; Schumm, J. S.; Tour, J. M. *J. Org. Chem.* **1997**, *62*, 1388−1410.

(35) Murray, C. B.; Kagan, C. R.; Bawendi, M. G. *Annu. Rev. Mater. Sci.* **2000**, *30*, 545−610.

(36) Brousseau, L. C.; Novak, J. P.; Marinakos, S. M.; Feldheim, D. L. *Adv. Mater.* **1999**, *11*, 447−449, 427.

(37) Novak, J. P.; Feldheim, D. L. *J. Am. Chem. Soc.* **2000**, *122*, 3979−3980.

(38) Novak, J. P.; Brousseau, L. C.; Vance, F. W.; Johnson, R. C.; Lemon, B. I.; Hupp, J. T.; Feldheim, D. L. *J. Am. Chem. Soc.* **2000**, *122*, 12029−12030.

(39) McConnell, W. P.; Novak, J. P.; Brousseau, L. C.; Fuierer, R. R.; Tenent, R. C.; Feldheim, D. L. *J. Phys. Chem. B* **2000**, *104*, 8925−8930.

(40) Deans, R.; Kim, J.; Machacek, M. R.; Swager, T. M. *J. Am. Chem. Soc.* **2000**, *122*, 8565−8566.

(41) Herz, L. M.; Silva, C.; Phillips, R. T.; Setayesh, S.; Mullen, K. *Chem. Phys. Lett.* **2001**, *347*, 318−324.

(42) Cornil, J.; dosSantos, D. A.; Crispin, X.; Silbey, R.; Bredas, J. L. *J. Am. Chem. Soc.* **1998**, *120*, 1289−1299.

(43) Beljonne, D.; Cornil, J.; Silbey, R.; Millie, P.; Bredas, J. L. *J. Chem. Phys.* **2000**, *112*, 4749−4758.

(44) Conwell, E. M. *Phys. Rev. B*: *Condens. Matter* **1998**, *57*, 14200−14202.

(45) Nguyen, T. Q.; Doan, V.; Schwartz, B. J. *J. Chem. Phys.* **1999**, *110*, 4068−4078.

(46) Lakowicz, J. R. *Principles of fluorescence spectroscopy*, 2nd ed.; Kluwer Academic/Plenum: New York, 1999.

(47) Schmelz, O.; Mews, A.; Basche, T.; Herrmann, A.; Mullen, K. *Langmuir* **2001**, *17*, 2861−2865.

(48) Norris, D. J.; Bawendi, M. G. *Phys. Rev. B: Condens. Matter* **1996**, *53*, 16338−16346.

(49) Shuai, Z.; Bredas, J. L. *Phys. Rev. B: Condens. Matter* **1995**, *52*, 13730−13733.

(50) Meulenberg, R. W.; Strouse, G. F. *J. Phys. Chem. B* **2001**, *105*, 7438−7445.

(51) Basko, D. M.; Agranovich, V. M.; Bassani, F.; La Rocca, G. C. *Physica Status Solidi A—Appl. Res.* **2000**, *178*, 69−72.

(52) Ruseckas, A.; Namdas, E.; Theander, M.; Svensson, M.; Yartsev, A.; Zigmantas, D.; Andersson, M. R.; Inganas, O.; Sundstrom, V. *Synth. Met.* **2001**, *119*, 603−604.